Comparison of Model-based Vs. Data-driven Methods for Fault Detection and Isolation in Engine Idle Speed Control System

Ruochen Yang[1,2], Giorgio Rizzoni[1,2,3]

[1]*Center for Automotive Research, Columbus, Ohio, 43212, USA*

[2]*Electrical and Computer Engineering, The Ohio State University, Columbus, Ohio, 43212, USA*

[3]*Mechanical and Aerospace Engineering, The Ohio State University, Columbus, Ohio, 43212, USA*

yang.1359@osu.edu
rizzoni.1@osu.edu

ABSTRACT

An internal combustion engine operating at idle is regulated by a feedback controller so that it runs at a preset idle speed without stalling when no acceleration is requested from the driver. Idle speed control is affected by numerous disturbances, ranging from accessory loads to environmental conditions. Because of the regulating behavior of the controller, faults, especially actuator faults, may affect sensor measurements in a way very similar to disturbances, system uncertainty or noise. This poses a challenge to the fault detection and isolation (FDI) problem for this system. In this paper, two fundamentally different fault diagnoses approaches are used to detect and isolate faults. A model-based residual generation scheme as well as a data-driven linear discriminant analysis scheme is developed to solve the FDI problem even when faults are concurring in addition to system uncertainty, disturbance and noise. Their performances are compared side by side using data gathered from an experimentally validated simulator for an engine idle system that considers an actuator fault, a sensor fault, several system uncertainties and disturbance (operating conditions), and sensor noise. The results show that comparable performance can be achieved with both schemes and some comments are made about each approach.

1. INTRODUCTION

Model-based fault diagnosis has been conventionally used in automotive applications (Isermann, 2005; Rizzoni, Onori, & Rubagotti, 2009), while data-driven diagnosis has become more popular in recent years. Research has been done to improve FDI performances by implementing one or a combination of the two for automotive systems (Mohammadpour, Franchek & Grigoriadis, 2011; Luo, Namburu, & Pattipati, 2010). However, few have studied the performance of each method applied on the same system to analyze the advantages and disadvantages of each method. This paper will demonstrate traits of each approach via an example on an internal combustion engine operating at idle speed.

For many years, the automotive industry has complied with on-board diagnosis (OBD) standards (SAE J1979, 2012), which require continuous monitor of various vehicle subsystem performances and the ability to store and report self-diagnostic results. Among the subsystems that must be diagnosed is the idle speed control system. We chose this example to illustrate two diagnostic approaches.

An idle speed controller stabilizes the engine operation at predetermined set points in accordance with its known working conditions, such as altitude and humidity, engine coolant temperature, transmission state, etc. (Okubo & Michelini, 2004). For instance, an engine that starts cold may have an increased idle speed set point to shorten the catalyst warm up time (Eriksson & Nielsen, 2014). However, unpredicted circumstances may cause the engine speed to fluctuate around such set points. Assume for example that the air conditioner compressor is turned on while the engine is idling: the engine is asked to provide an external load torque. Before the controller can react, the engine speed drops dramatically to compensate for the torque request. Based on sensor measurements, the controller brings the idle speed back to the set point by

calculating a different value for the idle air control (IAC) valve setting. In this project, we consider faults in IAC valve and in pressure sensor, plus noise, system uncertainty and disturbance.

We then test and evaluate both model-based algorithm, as well as a data-driven one, to perform FDI under all possible operating conditions. Section 2 defines the FDI problem and explains the engine system, faults, uncertainties and disturbance. Section 3 and 4 present a model-based and a data-driven FDI scheme respectively and their results. Section 5 shares some comments for each approach and thoughts that come up during the design process.

2. SYSTEM BACKGROUND

2.1. Description of the System

Table 1 explains every mathematical symbol that is used to model the engine system. Known values are also indicated in the table except a_i, $i=1...14$, the coefficients of fitted functions based on experimental validation data.

The system of an engine operating at an idle speed of 800rpm is a nonlinear system and Figure 1 shows its block diagram. The system has 1 known input θ_{cmd} and 2 sensor measurements y_1 and y_2 as outputs. Both measurements contain additive white Gaussian noise and the signal-to-noise ratio is 57dB for pressure sensor and 46dB for speed. Two possible faults are the IAC valve actuator fault and the pressure sensor fault. T_{dist} is an external load torque requested from the engine and is treated as a disturbance. The system has parameter uncertainties in the intake manifold dynamics and the friction model. The goal for the FDI algorithms is to detect and isolate the two faults with known variables (1 valve opening command and 2 sensor measurements) in the presence of uncertainty, disturbance and noise.

This project uses data generated by an experimentally validated simulator, developed at the Center for Automotive Research at The Ohio State University. The model described by the simulator gives good approximation of real system when engine speed is below 1400rpm and IAC valve position is below 15% open (Rizzoni, 1995-2016).

The engine idle speed controller sends an opening command to the valve. The valve actuator may have a bias fault and the actual opening position may be greater than the commanded value. The mass flow rate across the throttle is considered as a choked flow when the valve position is below 15%. It is estimated as a polynomial function of the IAC valve position.

Table 1. Symbols and Definitions.

Variable	Definition
θ_{cmd}	Commanded IAC valve opening position
θ_{act}	Actual throttle valve opening position
m, $\dot{m}$	Air mass in the intake manifold, air mass flow rate in the intake manifold
$\dot{m}_{thr}$	Throttle valve air mass flow rate
$\dot{m}_{port}$	Port air mass flow rate
P_0	Ambient pressure, 99.79kPa
T_0	Ambient temperature, 298K
R	Gas constant of air, 287J/(kg*K)
k	Specific heat ratio of air, 1.4
V_d	Engine displacement, 0.00379m^3
N	Rotational engine speed
P_m	Intake manifold pressure
T_m	Intake manifold temperature
V_m	Intake manifold volume, 0.0029 m^3
T_{ind}	Indicated torque
AF	Air-fuel (AF) ratio, 14.6
θ_{spk}	Spark timing, 10 °before top dead center
T_{dist}	Disturbance, the external load torque
$T_{fri+dist}$	Sum of disturbance and amount of friction torque above nominal
J	Rotational inertia of the engine, 0.0789Nm*sec/(rad/sec)
a_i, $i=1...14$	Fitted function coefficients based on experimental engine data, known values
f_{thr}	IAC valve actuator fault
f_p	Intake manifold pressure sensor fault
y_1	Intake manifold pressure sensor measurement
y_2	Engine speed sensor measurement

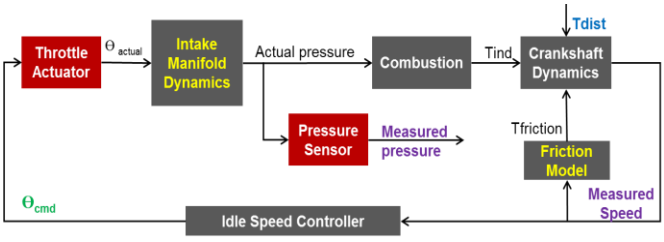

Figure 1. Engine System Block Diagram.

Following a filling-and-emptying approach, the intake manifold dynamics are modelled as a mass neglecting heat exchange. The intake manifold temperature's state equation is modelled as a function of intake air mass, and the air flow rate through the throttle and port. Neglecting the scavenge

flow, the port air mass flow rate is evaluated via a speed-density equation, which is approximated as a function of engine speed and intake manifold pressure.

In the combustion model, the indicated torque is calculated as a function of the port air mass flow rate, AF ratio and spark timing. The model also considers a combustion delay correlated to the engine speed. In this project, the AF ratio and spark timing are treated as constants.

The rotational dynamics of the engine crankshaft is evaluated as a lumped-parameter model with one degree of freedom. The friction torque is estimated as a polynomial function of the engine speed and the coefficients are varying depending on whether the engine has been warmed up. A mathematical system model is presented in Section 2.3.

2.2. Description of Simulation Configuration

In this paper, we generate virtual data by simulations. To mimic more realistic conditions, noise and uncertainties are included as explained below. Two thousand 2-minute simulations are run with 5ms/sample step size for detector validation and testing. Figure 2 presents sample plots from a simulation. All simulations imitate an engine with idle speed set point of 800rpm, starting cold and warming up linearly over a 1-minute period. The resulting friction load starts from a higher value and decreases to its nominal in a minute. Since in reality it is unknown whether the engine starts warm, there is an uncertainty in friction. The simulator models intake manifold temperature dynamics and engine friction using physics-based (nonlinear) models. In the model-based algorithms introduced in Section 3, the linearized model is simplified to permit the development of algorithms that can be readily implemented.

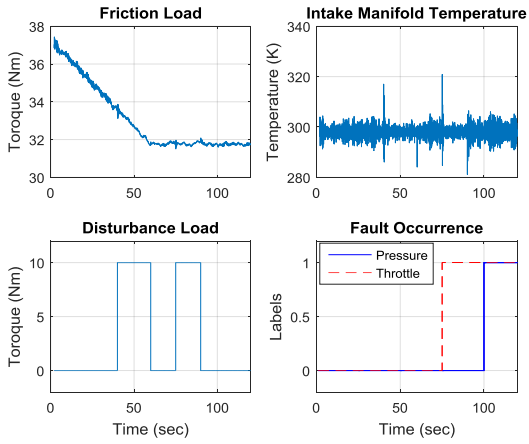

Figure 2. Sample plots from 1 simulation.

Disturbance load is injected as an intermittent 10Nm torque to resemble an air compressor working on and off, whose duration and injection time is randomized. Each simulation contains at least 1, at most 2 pulses. Faults are injected to the system randomly and once injected, affected components stay faulty. A simulation may have 0, 1 or 2 faults that appear in random order. Both faults are bias faults that increase the valve opening command by 5% of its nominal value and the pressure sensor measurement by 8% of its nominal. The corresponding intake manifold temperature profile is demonstrated in Figure 2. It varies based on the randomized operating condition, but without information of these conditions, the temperature is considered as a constant and therefore introduces uncertainty. No fault/disturbance is injected within the first 2 seconds for the simulator to stabilize and only data from 2-120s are collected and plotted throughout this paper.

Figure 3 plots the known variables in a simulation for a healthy case versus a faulty case. The configuration for the healthy one: 1) engine starts from cold, 2) disturbances injected during 40-60s and 75-90s, 3) no faults, 4) measurements contain noise. The configuration for the faulty: 1) engine starts from cold, 2) disturbances injected during 40-60s and 75-90s, 3) valve actuator fault injected starting from 20s, pressure sensor fault injected starting from 80s, 4) measurements contain noise. Comparing the healthy and faulty plots in Figure 3, it is obvious that faults can't be easily detected and identified.

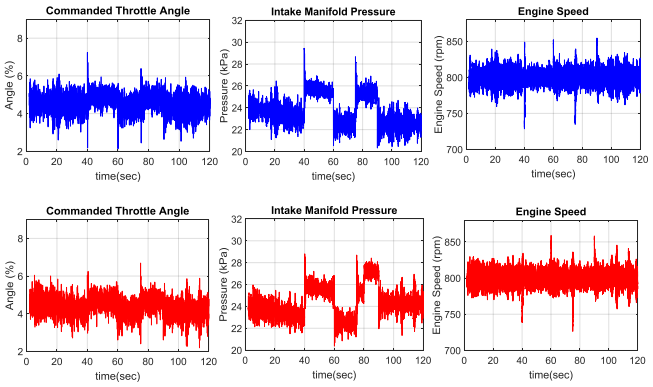

Figure 3. Healthy (Top) Vs. Faulty (Bottom) Scenario.

A separate training data set is acquired in a similar fashion for the data-driven scheme. The same configuration in friction load, intake manifold temperature and volumetric efficiency apply. The only difference is that faults and disturbances are not injected randomly. System health is divided into 4 classes: healthy, single throttle fault, single pressure fault, and both faults. 800 simulations are generated for each class, which half of it contains a constant 10Nm disturbance and others do not. Every simulation keeps the same configuration from 2-120s, i.e. a simulation for throttle fault with disturbance has the fault and disturbance injected from 2s till 120s.

2.3. Structural Analysis

Structural analysis (Blanke & Schroder, 2003) investigates the structural properties of a dynamic model by analysing its structural model. It is a very useful tool to identify which

part of the system is monitorable (i.e. the subset of the system components whose faults can be detected and isolated), provide information about the analytic redundancy of the system which can be used to design residuals, and determine those components whose failure can be tolerated through reconfiguration (i.e. sensor placement) (Krysander & Frisk, 2008).

The engine system without controller can be represented in the following equations based on the assumptions descripted in the previous section:

$$e_1: \theta_{act} = \theta_{cmd} + f_{thr}$$
$$e_2: \dot{m} = \dot{m}_{thr} - \dot{m}_{port}$$
$$e_3: \dot{m}_{thr} = P_0\sqrt{\frac{k}{RT_0}}\sqrt{(\frac{2}{k+1})^{\frac{k+1}{k-1}}}(a_1\theta_{act}^2 + a_2\theta_{act} + a_3)$$
$$e_4: \dot{m}_{port} = \frac{V_d N}{120RT_m}(a_4 P_m - a_5)$$
$$e_5: \dot{T}_m = \frac{1}{m}(\dot{m}_{thr}(kT_0 - T_m) - \dot{m}_{port}(k-1)T_m)$$
$$e_6: P_m = \frac{mRT_m}{V_m}$$
$$e_7: T_{ind} = T_{int}(a_9 AF^2 + a_{10}AF + a_{11})(a_{12}\theta_{spk}{}^2 + a_{13}\theta_{spk} + a_{14})$$
$$e_8: T_{int} = a_6 P_m + a_7$$
$$e_9: \dot{N} = (T_{ind} - T_{fri+dist})\frac{30}{J\pi}$$
$$e_{10}: y_1 = P_m + f_p$$
$$e_{11}: y_2 = N$$

where $P_0, R, T_0, k, V_d, V_m, AF, \theta_{spk}, J, a_i,\ i = 1...14$ are known coefficients from the experimentally verified system model; $\theta_{act}, \dot{m}_{thr}, \dot{m}_{port}, m, P_m, T_m, T_{ind}, T_{int}, T_{fri+dist}, N, f_{thr}, f_p$ are unknown variables (Rizzoni, 1995-2016). Figure 4 summarizes the engine system as a structural incidence matrix of system variables vs. constraints, upon which Dulmage-Mendelsohn (DM) decomposition is performed.

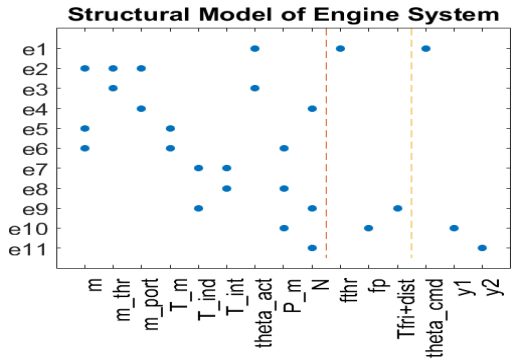

Figure 4. Engine System Structural Incidence Matrix.

DM-decomposition decomposes the incidence matrix into structural under-constrained, just-constrained, and over-constrained part (Dustegor, Frisk, Cocquempot, Krysander, & Staroswiecki, 2005). Analytic redundancy resides in the structural over-constrained part and therefore only faults occurring in this part can be detected. Furthermore, isolability test separates the over-constrained part into several equivalent classes, where faults appearing in the same class can't be isolated from each other even though they are detectable (Krysander & Frisk, 2008). Result from the DM-decomposition for the engine system is presented on left in Figure 5. It shows that this system model contains only structurally over-constrained subsystem, thus all faults/disturbance can be detected. Constraints e_1-e_6 form an equivalent class that contains the throttle valve actuator fault, while constraints e_7-e_9 form another that contains the lumped variable for the disturbance and the uncertainty in friction load $T_{fri+dist}$. e_{10} and e_{11}, each forms its own equivalent class and e_{10} contains the pressure sensor fault. Since all faults/disturbance appear in different classes, they are all detectable and isolable from each other, illustrated in the isolability matrix in Figure 5 on right. The analysis indicates that no additional sensors are needed to perform FDI for this system setup.

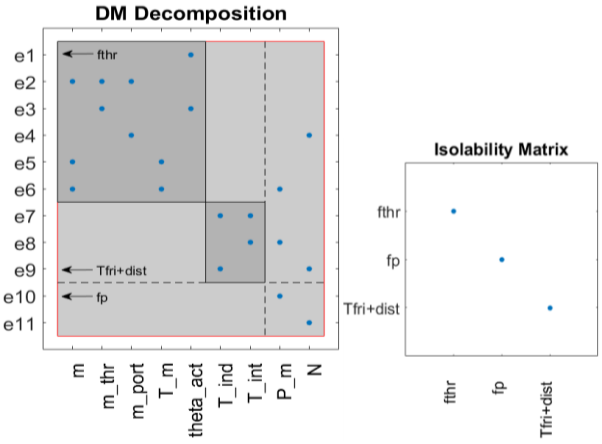

Figure 5. Structural Analysis Results.

3. MODEL-BASED FDI

An observer-based FDI scheme is designed in this section using a linearized system model. Behavior of the linearized model is studied against the nonlinear plant when healthy. Several observers are designed to generate residuals for robust FDI performance, which will be presented and discussed at the end of this section.

3.1. System Linearization

The original non-linear system without controller is analytically linearized around its nominal operating point, where $N = 800\text{rpm}$, $T_m = 298\text{K}$, $P_m = 22.462\text{kPa}$ and

$m = 0.76165\text{g}$. The state-space representation of the linearized healthy system is:

$$\begin{bmatrix} \dot{m} \\ \dot{N} \end{bmatrix} = A\begin{bmatrix} m \\ N \end{bmatrix} + B\begin{bmatrix} \theta_{cmd} + f_{thr} \\ 1 \end{bmatrix} + ET_{fri+dist}$$

$$\begin{bmatrix} P_m \\ N \end{bmatrix} = C\begin{bmatrix} m \\ N \end{bmatrix} + \begin{bmatrix} f_p \\ 0 \end{bmatrix}$$

where

$$A = \begin{bmatrix} -5.5482 & -4.5257e-6 \\ 1.2401e7 & -0.3349 \end{bmatrix},\quad B = \begin{bmatrix} 1.1257e-3 & 2.29154e-3 \\ 0 & -9.1775e3 \end{bmatrix}$$

$$E = \begin{bmatrix} 0 \\ -121.0304 \end{bmatrix},\qquad C = \begin{bmatrix} 2.9492e7 & 0 \\ 0 & 1 \end{bmatrix}$$

The states are *m*: the air mass in the intake manifold, and *N*: the engine speed. The inputs are θ_{cmd} : the known valve opening command from the controller, and a constant 1 which comes from the constant terms in the linearization. The unknown input, $T_{fri+dist}$, which may be present at random, is the sum of disturbance torque and amount of friction load above nominal. Figure 8 plots one realization of $T_{fri+dist}$ in red. The decreasing trend during the first 60s is stochastic and it simulates the extra friction load on the engine during warm-up. The pulses simulate the intermittent additional load torque due to accessories and each 120s simulation may contain 1 or 2 pulses. As both injection time and duration are random, the pulses may occur while engine warm-up. Outputs are the intake manifold pressure and the engine speed, P_m and *N*. When injected, f_{thr} is a constant of 0.219% valve opening and f_p is a constant of 1.797kPa; otherwise, zeros.

This linearized system contains several modelling errors due to system uncertainties besides linearization approximation error. It treats the volumetric efficiency, intake manifold temperature, and friction coefficients as constants, rather than dynamic values. In addition, sensor noise is not considered.

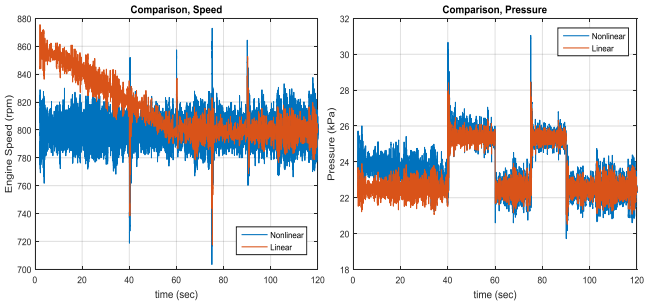

Figure 6. Comparison of Nonlinear Vs. Linear Plant.

Outputs from the linearized healthy plant are compared to the original in Figure 6 when noise, disturbance and uncertainty are present. During engine warm-up, the IAC valve is commanded to open up more in order to overcome additional friction load. Since the linearized model does not take into account the extra friction load torque, it gives greater engine speed and smaller intake manifold pressure than the nonlinear plant over the first 60sec warm-up period. Aside from the engine warm-up, Figure 6 confirms that the linearized system behaves very closely to the original system and the linearized the system will be used as the basis for the model-based FDI design.

By checking $rank(C*E) = rank(E)$ (Hui & Zak, 2005), there exists an unknown input observer (UIO) to estimate $T_{fri+dist}$. Since both the controllabiliy matrix and the observability matrix of the linearized system have full rank, the system is controllable and the states are observable. Hence, intuitively, the lumped variable for disturbance and uncertainty in friction load, $T_{fri+dist}$, may be detected via UIO and be isolated from the faults; the intake manifold pressure sensor fault, f_p , and the valve actuator fault, f_{thr} , may be detected by comparing the differences between estimated and measured outputs of P_m and *N*. Agreeing with the structural analysis of Section 2, these results from a control perspective indicate all faults/disturbance can be detected. Indeed, the faults and disturbance can be isolated from each other as implied by structural analysis in Figure 5. The next section will show a residual generation framework for model-based FDI.

3.2. Observer-based Residual Generation

Based on the linearized system model, a residual generation and evaluation logic is developed to detect and isolate faults, illustrated in Figure 7. An UIO (Hui & Zak, 2005) utilizes all available information θ_{cmd}, P_m, N to estimate $T_{fri+dist}$, and the estimate $\hat{T}_{fri+dist}$, together with θ_{cmd}, N , is sent to a sliding mode observer (SMO) that produces estimated intake manifold pressure and engine speed, $\hat{P}_m$ and $\hat{N}$ (Drakunov & Utkin, 1995). A set of residuals, r_p and r_N , is achieved by subtracting the estimates from the nonlinear plant sensor measurements. For change detection, a CUSUM test corresponding to each residual renders a fault label decision continuously in time (Basseville & Nikiforov, 1993).

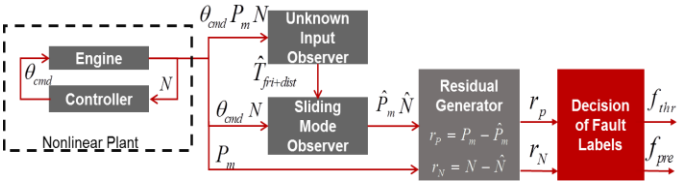

Figure 7. Residual Generation Flow Chart.

Figure 8 displays the actual $T_{fri+load}$ and the UIO result of its estimate $\hat{T}_{fri+load}$ in the faulty case simulation described in Figure 3. Note that it means, by definition, there is no additional load besides the nominal amount of friction when $T_{fri+load}$ is zero. The estimated load torque is noisy but it closely resembles the actual one.

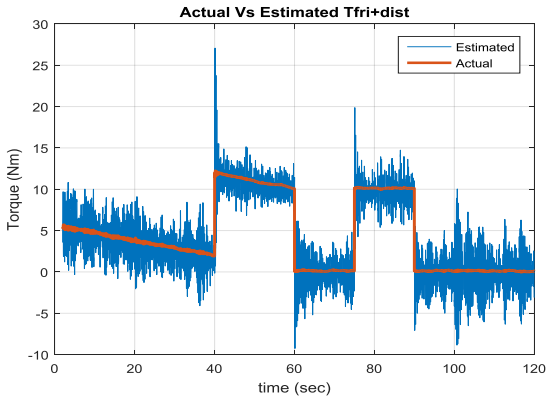

Figure 8. Estimated Vs. Actual $T_{fri+dist}$.

From the same simulation, Figure 9 plots the SMO estimates against their nonlinear plant sensor measurements. Fault injections are indicated as well: pressure sensor fault starts at 80s while throttle valve actuator fault has already been present since 20s. When the valve is faulty, it opens more than commanded and the controller tries to compensate it by sending a smaller θ_{cmd}. Since the SMO derives estimates from θ_{cmd}, it does not see the actuator fault. Similarly, the SMO does not see the pressure sensor fault because P_m is not used. Figure 9 illustrates the discrepancies between estimates and measurements when faults are present. Furthermore, a residual can be designed to identify valve actuator fault as $r_N = N - \hat{N}$, and another for pressure sensor fault as $r_P = P_m - P_m$.

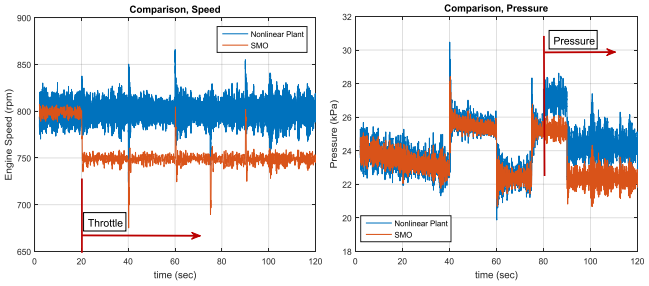

Figure 9. Estimated Vs. Actual Sensor Measurements.

Ideally, if a fault is absent, the corresponding residual is zero; otherwise, non-zero. Nevertheless, the noise, disturbance and uncertainty in the system make it stochastic. Residual distributions are fitted with normal distributions, which imply that prior knowledge of the residuals is required. Here, 1000 simulations are used for threshold tuning and validation of the detector, while the other 1000 are used for testing. Figure 10 displays the residuals from the same simulation as in Figure 9, and the fitted probability density functions under healthy and faulty condition. Distributions of r_p have very little overlap and little detection error is expected. On the other hand, distributions of r_N have larger overlap and a greater confusion is expected.

Established on the residual PDF's, a CUSUM (cumulative sum) test is built for r_p to detect pressure sensor fault and another for r_N to detect throttle actuator fault. It calculates the log-likelihood ratio of a data sequence until a threshold is reached. Proper thresholds are determined during tuning/validation stage to achieve appropriate detection performance.

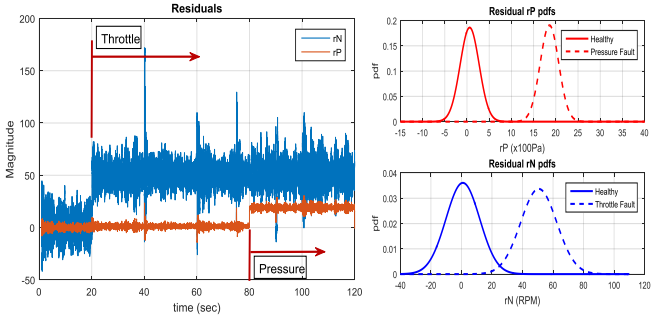

Figure 10. Residuals and Corresponding Distributions.

3.3. Results from Model-Based FDI Scheme

In this project, false alarms are defined as detections before true occurrence time or detections when truly no fault occurs; detections are defined as detections with a delay less than 5 seconds.

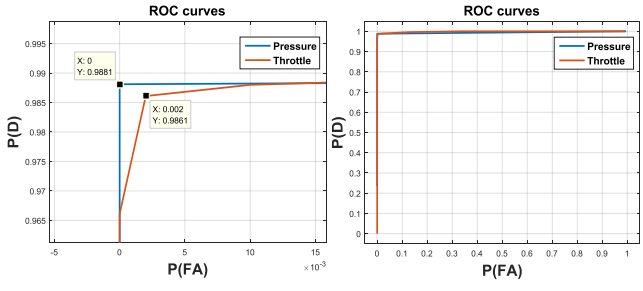

Figure 11. ROC Curves for Each Detector (Right), Zoomed-in Plot of the Northwest Corner (Left).

The Receiver Operating Characteristic curves of the detectors are plotted in Figure 11 based on the validation process using 1000 simulations. The thresholds that deliver optimal results (minimum average error) correspond to the points at the northwest-most corner. The final detectors set

such thresholds and are tested on the other 1000 simulations. The detector for pressure sensor fault accomplished 100% detection rate and 0% false alarm; and for throttle actuator fault, 100% detection rate and 4.6% false alarm.

4. DATA-DRIVEN FDI

Via linear discriminant analysis (LDA), a similarity-based classifier is designed in this section. Even though transient behavior exists from fault/disturbance injection, the engine speed variations are small because the controller stabilizes the engine at 800rpm. Hence, speed measurements are not as meaningful as the other two available variables for the FDI tasks in this project. Only the commanded throttle position and intake manifold pressure measurement, θ_{cmd} and P_m, are used for the data-driven FDI scheme, even though P_m itself may have a sensor fault.

4.1. Training Data Analysis

The training data set is clustered into 4 classes: 1. Healthy (and/or disturbance), 2. one Throttle fault (and/or disturbance), 3. one Pressure fault (and/or disturbance), 4. both faults (and/or disturbance). Training data, $[P_m, \theta_{cmd}]$, from each class (400 simulations each) are segmented into overlapping frames, 0.5s/frame and 0.25s/increment, and the mean of each frame is calculated.

Figure 12 illustrates the obtained clusters for each class labeled by color on left. Each class consists of two clusters: condition without disturbance on the lower left side, and with disturbance on the upper right. Four solid color dots represent the center of mass for each class. Figure 12 also presents the fitted PDF of each class when projected onto one of the original axes, pressure or throttle command. It is obvious that several distributions completely overlap even though they denote different health conditions. In other words, neither original axes offer good separation between classes.

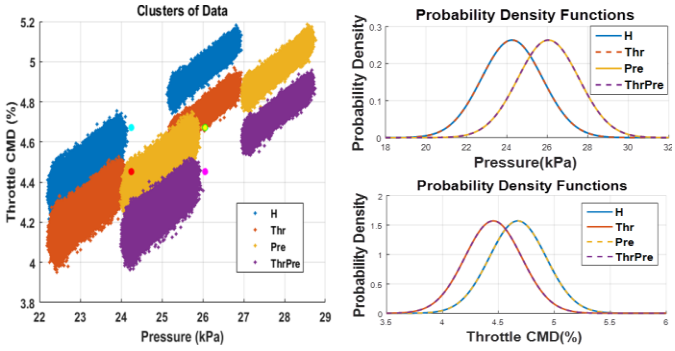

Figure 12. Clusters of Class Based on Mean Values and Their Distributions.

It is desirable to find a projection such that the separation between means of projected classes is maximized and the variance within each projected class is minimized. The first thing that comes to mind is LDA. The solution can be attained by calculating eigenvectors based on the between-class and the within-class covariance matrices, as described in the book from Hastie, Tibshirani and Friedman (2009). Figure 13 demonstrates the clusters after LDA, where the new axes are the two 1-D subspaces defined by the eigenvectors. It also depicts the fitted PDF of each class when projected onto each discriminant. Best separation occurs when data is projected onto Discriminant 1 according to Figure 13. The corresponding transformation is adopted by the classifiers in the data-driven FDI method.

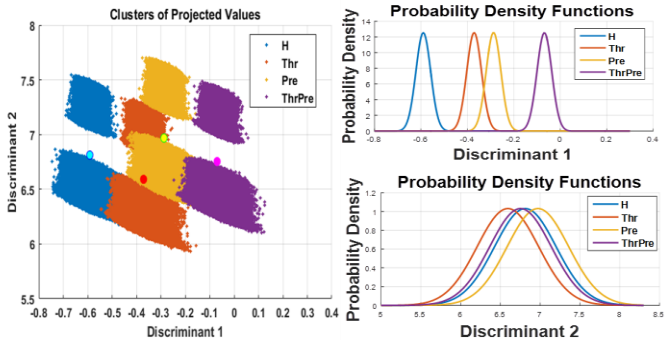

Figure 13. Clusters after LDA and Their Distributions.

4.2. Detection Logic

Without knowledge of the physical engine model, a fault diagnostic procedure is constructed using only the commanded throttle opening and the measured intake manifold pressure, which could be faulty.

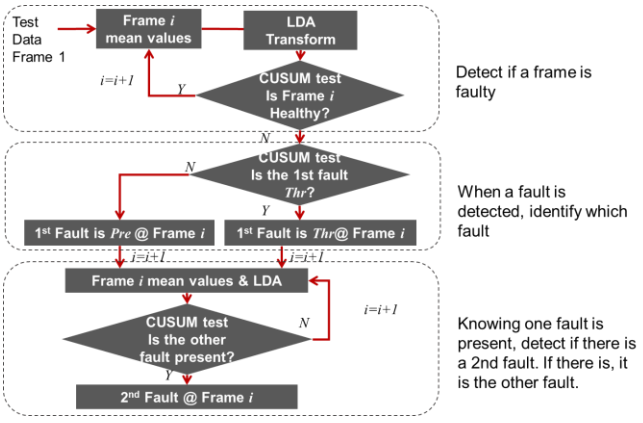

Figure 14. Model-free FDI Flow Chart.

Figure 14 lays out the procedure for a test sequence. Similar to the training data, a test sequence is parsed into overlapping frames and the previously acquired projection transforms the mean P_m and θ_{cmd} onto Discriminant 1. A CUSUM based classifier detects whether the frame is

generated by a healthy system through fitted distributions of healthy vs. non-healthy training data. Once a non-healthy frame is detected, another CUSUM test identifies whether it is a single throttle fault or a single pressure fault. Knowing that a first fault has arisen, the algorithm moves on to the next frame and check if the other fault occurs until end of sequence.

4.3. Results from Data-Driven FDI Scheme

For easy comparison with model-based approach, false alarms and detections are defined the same as in Section 3.3, and the same set of validation and testing data is used here. The ROC curves corresponding to each fault are plotted in Figure 15 after validation using 1000 simulations. Similarly, the finalized algorithm sets thresholds corresponding to the points at the northwest-most corner and it is tested on the other 1000 simulations. Comparable to results from the model-based algorithm, the detection rate of pressure sensor fault is 99.04% and false alarm rate, 0%; the detection rate of throttle actuator fault is 99.8% and false alarm rate, 0.8%.

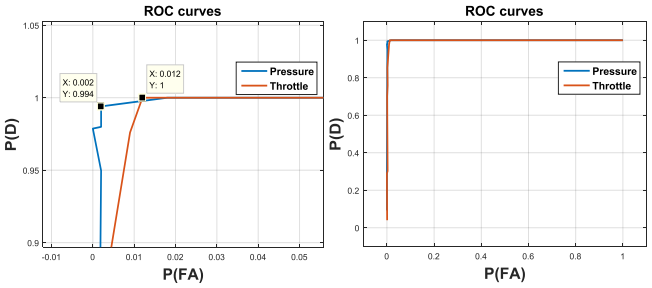

Figure 15. ROC Curves for Each Detector (Right), Zoomed-in Plot of the Northwest Corner (Left).

5. COMMENTS

Table 2 summarizes the FDI performance of the model-based framework as well as the data-driven one. Both methods developed in this paper deliver similar and satisfactory fault diagnostic performance for the engine system setup. This section comments on some of their advantages and shortcomings during the design and application process.

The system model makes it possible to conduct structural analysis, which is meaningful in the early stage of FDI design. It offers insight of whether faults can be detected and isolated, or whether they can be made so by way of a different sensor placement. On the other hand, before the design stage, it is usually not clear to a data-driven method whether faults and disturbances are detectable or isolable, much less to determine which variables should be monitored for efficient fault diagnosis.

With knowledge of the physical model, observer-based method is able to estimate system parameters and is able to uncover useful information that is not known or measured (Isermann, 2005). But, modeling error, as well as linearization error, can limit its performance. A complete separate study can be done to assess its sensitivity and robustness to fault, disturbance and modeling error.

Nonetheless, modeling errors do not concern the data-driven method because it does not depend on the model and uses only the available data. However, whether training data is balanced and sufficient can be critical (Rizzoni et al, 2009). In addition, certain techniques can be more effective than others depending on the application. It is useful to understand how the data spread beforehand, even though it might still need some trial and error. For instance, during the course of developing the data-driven scheme in this paper, Gaussian Mixture Model (GMM) and Principal Component Analysis (Hastie et al 2009) are also applied to perform classification for fault diagnosis in this engine system. Unfortunately, their performance is not better than what has been presented. Moreover, GMM especially adds considerable computation complexity and memory consumption.

Table 2. Comparison of Performances.

Observer-based Residual Generation			
Fault	Rates	Validation Set	Test Set
Valve Actuator Fault	False Positive (%)	1.2	0.8
	Detection (%)	100	99.8
Pressure Sensor Fault	False Positive (%)	0.2	0
	Detection (%)	99.4	99.04
Model-free Linear Discriminant Analysis			
Fault	Rate	Validation Set	Test Set
Valve Actuator Fault	False Positive (%)	1.2	0.8
	Detection (%)	100	99.8
Pressure Sensor Fault	False Positive (%)	0.2	0
	Detection (%)	99.4	99.04

6. CONCLUSION

This paper demonstrates two dramatically different fault diagnostic methods, model-based vs. data driven, to solve the same FDI problem in an engine operating at idle. Their results are similar and both methods are able to give high detection rate while keeping very small false alarm rate. Strengths and weaknesses of each method are compared. Even though the performance is analyzed using virtual data from an experimentally validated simulator, we believe that the guidance provided by this study would be a useful starting point in the design of practical DFI strategies in an industrial application.

REFERENCES

Isermann, R. (2005). Model-based fault and diagnosis – status and applications. *Annual Reviews in Control*, 29 (1),71-85. doi:10.1016/j.arcontrol.2004.12.002

Rizzoni, G., Onori, S., & Rubagotti, M. (2009). Diagnosis and prognosis of automotive systems: motivations, history and some results. *Proceedings of the 7th IFAC Symposium on Fault Detection, Supervision and Safety of Technical Processes* (191-202), June 30 – July 3, Barcelona, Spain. doi:10.3182/20090630-4-ES-2003.00032

Mohammadpour, J., Franchek, M., & Grigoriadis, K. (2011). A Survey on Diagnostics Methods for Automotive Engines. *Proceedings of the 2011 American Control Conference* (984-990), June 29 – July 01, San Francisco, CA. doi:10.1109/ACC.2011.5990643

Luo, J., Namburu, M., & Pattipati, K. R. (2010). Integrated model-based and data-driven diagnosis of automotive antilock braking systems. *IEEE Transactions on Systems, Man, and Cybernetics—Part A: Systems and Humans*, 40 (2), 321-336. doi:10.1109/TSMCA.2009.2034481

Okubo, C., & Michelini, J. *Idle speed control method and system*. Patent US 2004/0074473 A1. 22 Apr. 2004. Print.

Eriksson, L., & Nielsen, L. (2014). *Modeling and Control of Engines and Drivelines*. West Sussex, UK: Wiley.

Rizzoni, G. *Coursenotes for ME7236, Powertrain dynamics, The Ohio State University*. 1995-2016.

Blanke, M., & Schroder, J. (1st Ed.). (2003). *Diagnosis and fault-tolerant control*. New York, NY, USA: Springer.

Krysander, M., & Frisk, E. (2008). Sensor placement for fault diagnosis. *IEEE Transactions on Systems, Man, and Cybernetics—Part A: Systems and Humans*, 38 (6), 1398-1410. doi: 10.1109/TSMCA.2008.2003968

Dustegor, D., Frisk, E., Cocquempot, V., Krysander, M., & Staroswiecki, M. (2005). Structural analysis of fault isolability in the DAMADICS benchmark. *Control Engineering Practive*, 14 (6), 597-608. doi:10.1016/j.conengprac.2005.04.008

Drakunov, S., & Utkin, V. (1995). Sliding mode observers. Tutorial. *Proceedings of the 34th IEEE Conference on Decision and Control*, (3376-3378), December 13-15, New Orleans, LA. doi:10.1109/CDC.1995.479009

Hui, S. & Zak, S. (2005). Observer design for systems with unknown inputs. *International Journal of Applied Mathematics and Computer Science*, 15 (4): 431-446.

Basseville, M., & Nikiforov, I. (1st Ed.). (1993). *Detection of abrupt changes: theory and application*. USA: Prentice Hall.

Hastie, T., Tibshirani, R. & Friedman, J. (2nd Ed.). (2009). *The elements of statistical learning*. New York, NY, USA: Springer.

SAE Standard J1979: E/E Diagnostic Test Modes (2012). *SAE International*. USA. https://saemobilus.sae.org/content/j1979_201202

BIOGRAPHIES

Ruochen Yang is a PhD student in Electrical and Computer Engineering and a Graduate Research Associate at the Center for Automotive Research at the Ohio State University. Her research interest is in fault diagnosis and prognosis in automotive applications.

Giorgio Rizzoni the Ford Motor Company Chair in Electromechanical Systems, is Professor of Mechanical and Aerospace Engineering and of Electrical and Computer Engineering, and Director of the Center for Automotive Research at the Ohio State University. He is a Fellow of IEEE and SAE. His research activities are related to modeling, control and diagnosis of advanced vehicles, energy efficiency, alternative fuels, the interaction between vehicles and the electric power grid, vehicle safety and intelligence, and policy and economic analysis of alternative fuels and vehicle fuel economy. He received BS, MS and PhD degrees in Electrical and Computer Engineering from the University of Michigan in 1980, 1982 and 1986.